PERGAMON

International Journal of Solids and Structures 40 (2003) 3425–3437

INTERNATIONAL JOURNAL OF SOLIDS and STRUCTURES

www.elsevier.com/locate/ijsolstr

Comparison of finite element techniques for 2D and 3D crack analysis under impact loading

M. Enderlein *, A. Ricoeur, M. Kuna

Institute of Mechanics and Fluid Dynamics, Technische Universität Bergakademie Freiberg, Lampadiusstrasse 4, Freiberg 09596, Germany

Received 16 July 2002; received in revised form 5 February 2003

Abstract

For several technical applications the dynamic aspect in fracture mechanics cannot be neglected. When the reliability of components with macroscopic cracks has to be assessed, the consideration of dynamic effects may lead to much higher stress intensity factors than under static conditions. In this paper three different methods to calculate the dynamic stress intensity factor for the mode-I loading of stationary cracks are compared. Based on two- and three-dimensional finite element simulations, the dynamic stress intensity factor is computed with the dynamic J-integral, the modified crack closure integral and the displacement interpretation method. The theoretical fundamentals of all three methods are summarized in the paper and the numerical implementation is explained briefly. Results for different models are shown and compared to findings in the literature.

Keywords: Fracture; Dynamic fracture mechanics; Dynamic stress intensity factor; Dynamic J-integral; Modified crack closure integral; Finite element method

1. Introduction

For several engineering applications, such as the development of transport casks for dangerous loads, the assessment of safety, integrity and reliability with static stress analyses and experiments under static conditions is not sufficient. That means applications, where high-speed loads may act, causing premature failure of the structure. Especially for structures containing cracks such dynamic impacts are very dangerous, because they may lead to crack initiation, accelerated growth and unstable propagation of cracks. In order to minimise the risks of failure, the dynamic aspects have to be considered in the fracture mechanics assessment of such structures and components.

The purpose of dynamic fracture mechanics is to analyse the growth, arrest and branching of cracks in structures subjected to dynamic loads. Several experimental techniques, for instance the method of caustics

* Corresponding author.
E-mail address: marco.enderlein@imfd.tu-freiberg.de (M. Enderlein).

0020-7683/03/$ - see front matter © 2003 Elsevier Science Ltd. All rights reserved.
doi:10.1016/S0020-7683(03)00117-3

or the dynamic photoelasticity method, have been developed to investigate the crack tip fields. Since these methods have many limitations theoretical models in combination with computational and numerical methods are more useful. Mostly boundary element methods have been developed for the calculation of dynamic fracture quantities, for instance by Nishimura et al. (1987), Wen et al. (1999) or Fedelinski et al. (1996). Finite element simulations have been performed by Nakamura et al. (1986), Shih et al. (1986) and Nishioka (1995). In almost all these investigations the fracture quantities have been calculated by means of the J-integral. Alternate techniques have been rarely investigated in dynamic fracture mechanics. Moreover, the authors are aware of merely one three-dimensional problem treated in the literature, where the loads are not applied at the crack faces. This is the elliptical crack in a rectangular bar (Nishioka, 1995). A good overview of the state of the art has been given by Aliabadi (1995).

In this paper three computational methods are described to calculate the dynamic stress intensity factor $K_{\mathrm{I}}^{\mathrm{d}}$ for stationary cracks: (i) the J-integral method, (ii) the modified crack closure integral (MCCI) and (iii) the displacement interpretation method (DIM). They are based on finite element simulations assuming linear elastic material behaviour and have been applied to two- and three-dimensional problems. The results of the methods are compared to each other. Moreover, some results are contrasted with findings in the literature. Three-dimensional calculations are presented for an elliptical crack and for a central through-thickness crack in a rectangular bar. The aim is to validate the MCCI and the DIM techniques with respect to the J-integral, which is assumed to be the most accurate method but requiring the highest effort of implementation as well.

2. Methods for the calculation of dynamic fracture quantities

2.1. Two-dimensional dynamic J-integral

Considering a two-dimensional body with a crack oriented along the x_1-axis, the J-integral vector J_k^{d} can be derived from an energy balance within the domain A, shown in Fig. 1. With Γ as a closed contour around the crack tip it is found:

$$J_k^{\mathrm{d}} = \lim_{\Gamma \to 0} \int_{\Gamma} [(U+T)\delta_{kj} - \sigma_{ij} u_{i,k}] n_j \, \mathrm{d}\Gamma. \tag{1}$$

This equation is valid for linear elastic material and was derived by Atkinson and Eshelby (1968) and independently by Kostrov and Nikitin (1970) and Freund (1972). The quantities σ_{ij} and u_i are the Cartesian components of the stress tensor and the displacement vector, n_j is the unit vector normal to Γ pointing

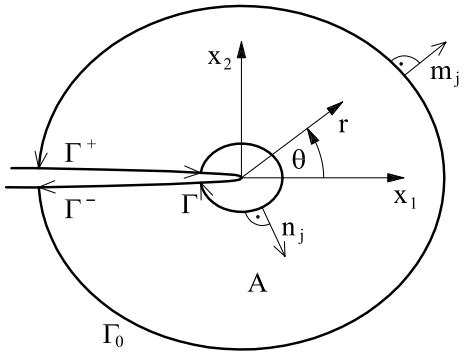

Fig. 1. Crack tip coordinates and integration contours.

outward of the enclosed domain and δ_{kj} is the unit tensor. $U = (1/2)\sigma_{ij}u_{i,j}$ denotes the specific elastic energy stored in the body and T means the kinetic energy density. Regarding only the x_1-component of J_k^{d}, which has the physical meaning of the energy release rate G, and restricting to the case of a stationary crack Eq. (1) reduces to

$$J_1^{\mathrm{d}} = G = \lim_{\Gamma\to 0}\int_{\Gamma}(U\delta_{1j} - \sigma_{ij}u_{i,1})n_j\,\mathrm{d}\Gamma. \tag{2}$$

To evaluate J_1^{d} with a finite element analysis, Eq. (2) is not suitable because the accurate calculation of fields in the region around the crack tip is very difficult. To circumvent these difficulties, Eq. (2) is transformed into a domain integral using the virtual crack extension technique (Shih et al., 1986; Hellen, 1975). Following this method, an arbitrary smooth weighting function q is introduced, which has the value one on the inner contour Γ and zero on the outer contour Γ_0 (see Fig. 1). This function q may be interpreted as the virtual displacement of a material point $(\bar{x}_1, \bar{x}_2)$ due to a unit virtual crack extension in x_1-direction (Nakamura et al., 1986). Using the weighting function q, Eq. (2) can be rewritten in the form:

$$J_1^{\mathrm{d}} = \lim_{\Gamma\to 0}\left[\int_C(\sigma_{ij}u_{i,1} - U\delta_{1j})m_j q\,\mathrm{d}C - \int_{\Gamma^+ + \Gamma^-}(\sigma_{ij}u_{i,1} - U\delta_{1j})m_j q\,\mathrm{d}C\right], \tag{3}$$

where $C = \Gamma + \Gamma^+ + \Gamma^- + \Gamma_0$. The vector m_j denotes the unit vector normal to C, pointing outward from the enclosed area A. Therefore, the vector n_j, which has been introduced for the derivation of Eqs. (1) and (2) is $n_j = -m_j$. Consequently, the signs have changed from Eq. (2) to Eq. (3). Applying the divergence theorem to the integral over C, using the equation of motion, assuming traction-free crack surfaces (the integral over $C^+ + C^-$ vanishes) and omitting body forces yields:

$$J = \int_A[(\sigma_{ij}u_{i,1} - U\delta_{1j})q_{,j} + \rho\ddot{u}_i u_{i,1}q]\,\mathrm{d}A. \tag{4}$$

2.2. Three-dimensional dynamic J-integral

For three-dimensional problems the J-integral needs to be evaluated along the crack front. It is assumed that the crack lies in the x_1–x_3-plane. A virtual crack extension is considered along a segment L_C of the crack front, whereby $\Delta l(s)$ defines the shape of the extended crack front at the position s (see Fig. 2). Introducing the dimensionless vector $l_k(s)$, whose norm varies between zero and one, $\Delta l(s)$ can be written as:

$$\Delta l(s) = \Delta a l_k n_k. \tag{5}$$

Here n_k is the unit normal vector at the crack front, which lies in the x_1–x_3-plane. The total energy release $-\Delta\Pi$ for this virtual extension amounts to:

$$-\Delta\Pi = \bar{J}^{\mathrm{d}}\Delta a = \int_{L_C} J^{\mathrm{d}}(s)\,\Delta l(s)\,\mathrm{d}s. \tag{6}$$

Introducing Eq. (5) gives:

$$\bar{J}^{\mathrm{d}} = \int_{L_C} J^{\mathrm{d}}(s)l_k(s)n_k\,\mathrm{d}s. \tag{7}$$

With $J^{\mathrm{d}}(s)n_k = J_k^{\mathrm{d}}$ we obtain:

$$\bar{J}^{\mathrm{d}} = \int_{L_C} l_k(s)\left[\lim_{\Gamma\to 0}\int_{\Gamma}(\sigma_{ij}u_{i,k} - U\delta_{kj})m_j\,\mathrm{d}\Gamma\right]\mathrm{d}s = \lim_{S_\Gamma\to 0}\int_{S_\Gamma}(\sigma_{ij}u_{i,k} - U\delta_{kj})m_j l_k(s)\,\mathrm{d}S, \tag{8}$$

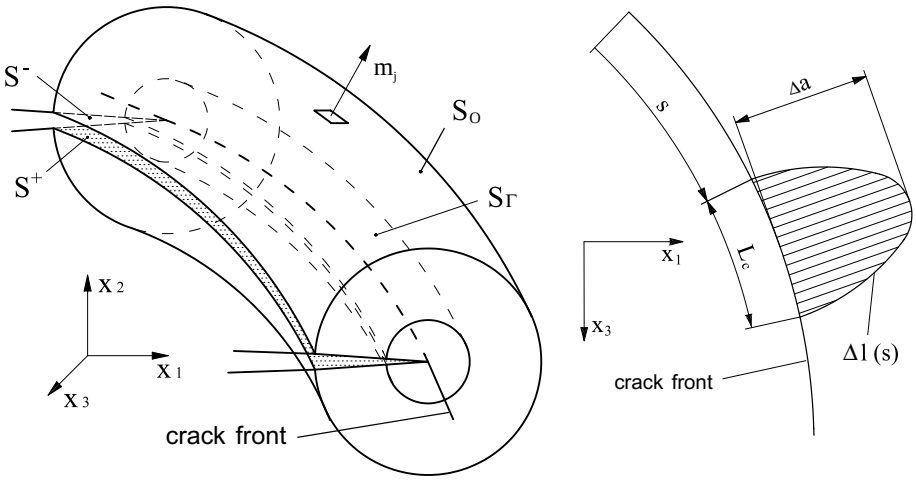

Fig. 2. Three-dimensional integration contours and virtual crack extension.

where S_Γ denotes the surface enclosing the crack front segment, as shown in Fig. 2. To obtain an average value of the J-integral, $J^{\mathrm{d}}(s)$ is assumed to be constant over the length L_C and thus can be excluded from the integration in Eq. (7) (Shih et al., 1986; Moran and Shih, 1987). Together with Eq. (8) this yields a J^{d} value, which is attributed to the middle point s^* of L_C:

$$J^{\mathrm{d}}(s^*) = \frac{\bar{J}^{\mathrm{d}}}{\int_{L_C} l_k(s) n_k \,\mathrm{d}s}. \tag{9}$$

To allow for an efficient finite element evaluation, Eq. (8) is now transformed into a volume integral. Similar to the procedure described in Section 2.1, a weighting function q is introduced which varies between one on the contour S_Γ and zero on S_0. With $q_k = q l_k(s)$ the weighting function becomes a vector and Eq. (8) can be rewritten as:

$$\bar{J}^{\mathrm{d}} = \int_S (\sigma_{ij} u_{i,k} - U\delta_{kj}) m_j q_k \,\mathrm{d}S - \int_{S^+ + S^-} (\sigma_{ij} u_{i,k} - U\delta_{kj}) m_j q_k \,\mathrm{d}S, \tag{10}$$

where $S = S_\Gamma + S^+ + S^- + S_0$ (see Fig. 2). Applying the divergence theorem to the integral over S yields

$$\bar{J}^{\mathrm{d}} = \int_V [(\sigma_{ij} u_{i,k} - U\delta_{kj}) q_{k,j} + \rho \ddot{\boldsymbol{u}}_i u_{i,k} q_k] \,\mathrm{d}V, \tag{11}$$

where V is the domain with the boundary S. Eq. (11) is valid for a stationary crack with traction-free crack surfaces and without body forces.

2.3. Numerical discretisation of the J-integral

To evaluate the J-integral with a finite element analysis, the integrals Eqs. (4) and (11) have to be computed numerically, i.e. a weighted summation has to be performed over all integration points of all finite elements in the considered domain. According to Eq. (11) for the general three-dimensional case, $\bar{J}^{\mathrm{d}}$ can be written as:

$$\bar{J}^{\mathrm{d}} = \sum_{\text{elements}} \sum_{\text{ips}} [(\sigma_{ij} u_{i,k} - U\delta_{kj}) q_{k,j} + \rho \ddot{\boldsymbol{u}}_i u_{i,k} q_k] |\mathbf{J}| w. \tag{12}$$

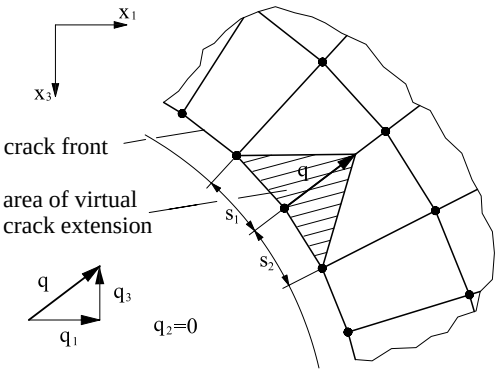

Fig. 3. Virtual crack extension and corresponding area ΔA.

Here $\mathbf{J}$ and w are the Jacobi matrix and the weight of the considered integration point. For the analyses discussed in this paper isoparametric four-node (2D) and eight-node elements (3D) with reduced integration were used (see Section 3.1). These elements have only one integration point in the centre of the local element coordinate system ($r_m = 0$). To calculate $\bar{J}^{\mathrm{d}}$ according to Eq. (12), all field variables have to be known at this point. Therefore, the values of $\ddot{u}_i$ and q_k have to be calculated at the integration point using the shape functions N^{α} for each node α:

$$\ddot{u}_i = \sum_{\alpha=1}^{8} N^{\alpha}(r_m)\ddot{u}_i^{\alpha}, \qquad q_k = \sum_{\alpha=1}^{8} N^{\alpha}(r_m)q_k^{\alpha}. \tag{13}$$

The calculation of the gradients $u_{i,k}$ and $q_{k,j}$ can be performed with the derivation of the shape functions in the local element coordinate system:

$$u_{i,k} = \frac{\partial r_m}{\partial x_k}\sum_{\alpha=1}^{8}\frac{\partial}{\partial r_m}N^{\alpha}(r_m)u_i^{\alpha}, \qquad q_{k,j} = \frac{\partial r_m}{\partial x_j}\sum_{\alpha=1}^{8}\frac{\partial}{\partial r_m}N^{\alpha}(r_m)q_k^{\alpha}, \tag{14}$$

whereby the derivation $\partial r_m/\partial x_k$ is the inverse of the Jacobi matrix $\mathbf{J}$. An important point in the calculation of $\bar{J}^{\mathrm{d}}$ is the distribution of the weighting function q. As stated in Section 2.1, q may be interpreted as a virtual crack extension. From the numerical point of view this means, that all nodes inside the integration region have to be shifted virtually ($q = 1$). For the nodes on the outer boundary and the nodes outside of the integration region, q has to be zero. In the three-dimensional case it has to be taken into account that q is a vector q_k. Therefore, all components of q_k need to be calculated depending on the actual position at the crack front. Furthermore, the integral in Eq. (9) needs to be calculated corresponding to the area ΔA of the virtual crack extension, depicted in Fig. 3.

2.4. Displacement interpretation method

The DIM is based on the evaluation of the crack tip near-field, which is of the same type for the static and the dynamic case (Gross, 1996). For mode-I the displacements u_2 show a $r^{1/2}$-behaviour at the positive (u^+) and the negative (u^-) crack faces, with a parabolic crack opening:

$$u_2^{\pm} = \pm\frac{K_{\mathrm{I}}}{2\mu}\sqrt{\frac{r}{2\pi}}(\kappa + 1) \tag{15}$$

Here K_I denotes the stress intensity factor for a mode-I crack opening, μ is the shear modulus and r the radial distance from the crack tip. For plane strain conditions κ is given by $\kappa = 3 - 4\nu$, where ν is Poisson's ratio. Since the crack tip field for spatial crack fronts is locally of the same type, Eq. (15) holds for 3D-mode-I problems, too (Anderson, 1995; Gross, 1996). In the finite element simulation K_I is calculated from Eq. (15) inserting the numerically calculated displacement u_2^+ from the node nearest to the crack tip. Since the accuracy of the numerical results in the vicinity of the crack tip is difficult to assess K_I values are alternatively calculated taking the displacement u_2^+ from several nodes along the crack face. The final value of K_I is determined by an extrapolation for $r \to 0$ and proved to fit well with the results from the node nearest the crack tip.

2.5. Modified crack closure integral

The crack closure integral is based on the method of the local energy release rate. The change of the total energy $-\Delta\Pi$ in a body due to a crack extension Δa is equal to the work that has to be done by the stresses on the crack faces in order to close the crack. For plane problems of thickness B the energy release rate G is defined as:

$$G = -\frac{1}{B}\frac{\mathrm{d}\Pi}{\mathrm{d}a} = -\lim_{\Delta a \to 0}\frac{\Delta\Pi}{B\,\Delta a}. \tag{16}$$

Assuming symmetry with respect to the crack plane, the energy release rate is calculated with the crack closure integral:

$$G = \lim_{\Delta a \to 0}\frac{1}{B\,\Delta a}\int_0^{\Delta a}\sigma_{2i}(s,0)u_i^+(\Delta a - s,\pi)\,\mathrm{d}s. \tag{17}$$

A polar coordinate system (r,θ) has been introduced (see Fig. 4) having its origin at the crack tip of the initial crack with the length a. In Eq. (17) the variable s specifies the location where the crack should be closed. Due to the assumption of an infinitely small Δa, Eq. (17) is exact. For a finite crack extension, the displacements would have to be taken from the grown crack. However, the MCCI technique gives an approximation of Eq. (17) for finite Δa, taking the stresses from the ligament and the displacements from the crack faces of the initial crack (Buchholz, 1984). Within the finite element context, Eq. (17) is numerically realised by multiplying the nodal forces in front of the crack tip with the corresponding displacements behind the crack tip (Buchholz, 1984). For a two-dimensional four-node element (see Fig. 4) this yields:

$$G = \frac{1}{BL}(F_i^{\alpha}u_i^{+\alpha-1}). \tag{18}$$

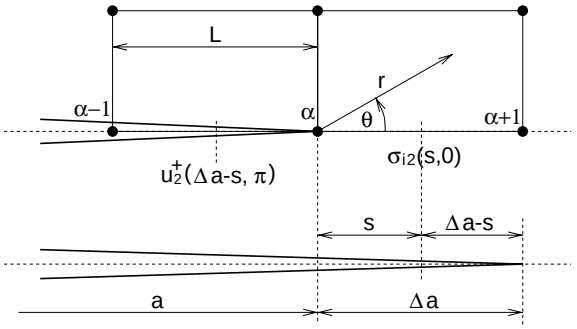

Fig. 4. MCCI technique.

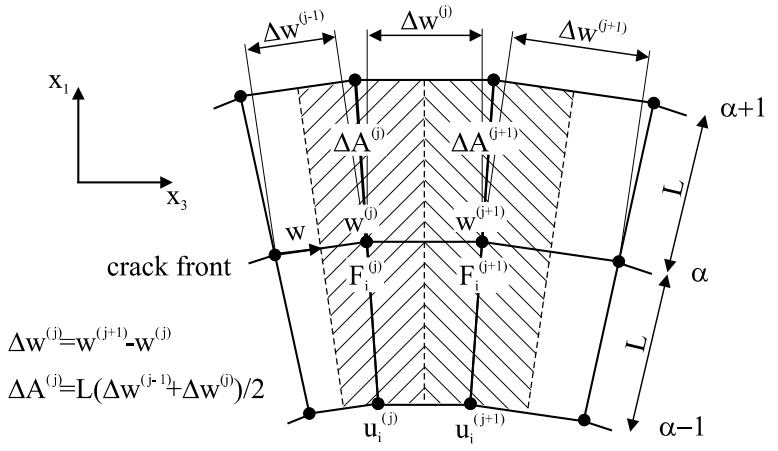

Fig. 5. Assignment of the areas of crack extension for a curved crack front.

If a three-dimensional crack configuration is considered, G is calculated along all nodes at the crack front. The crack extension $B\Delta a$ is replaced by local areas of crack extension $\Delta A^{(j)}$ at a crack front position $w^{(j)}$. The composition of $\Delta A^{(j)}$ is illustrated in Fig. 5 for a curved crack front, whereby the areas in front of the crack and behind it are different and have to be weighted.

$$G(w^{(j)}) = \frac{1}{\Delta A^{(j)}}(F_i^{(j)} u_i^{+(j)}). \tag{19}$$

3. Numerical examples

3.1. Central through-thickness crack in a rectangular bar, 2D-model

To compare the accuracy of the methods described in the previous section, several numerical examples are given in the following. For the solution of the boundary value problem the finite element solver ABAQUS/Explicit (2000) was used. This software works with an explicit time integration scheme, which in dynamic calculations shows clear advantages over implicit methods regarding the computation rate. Its efficiency is due to the use of diagonal mass matrices, which can be easily computed for first-order quadrilateral and hexahedral elements. The lower accuracy of these elements compared to higher-order elements can be compensated by far using a finer discretisation. Therefore, first-order elements are preferred in ABAQUS/Explicit (2000). The dynamic J-integral, the MCCI and the DIM are implemented as a post-processor.

The first example deals with a rectangular bar containing a central through-thickness crack. The model with its geometric properties is shown in Fig. 6. An impact load is applied at the opposite ends of the bar by $\sigma_0 H(t)$, where $H(t)$ is the Heaviside step function. The material constants are as follows: shear modulus $\mu = 76.92 \times 10^9$ Pa, density $\rho = 5000\ \mathrm{kg\,m^{-3}}$, Poisson's ratio $\nu = 0.3$. The two-dimensional finite element realisation of the model is shown in Fig. 7. A state of plane strain is assumed. Because of the symmetries with respect to the x_1–x_3-plane and the x_2–x_3-plane only a quarter of the bar was modeled. In order to study the influence of the mesh in the region around the crack tip two meshes with different fineness were analysed. For mesh (a) the ratio between the edge length $r_{\min}$ of the smallest elements at the crack tip and

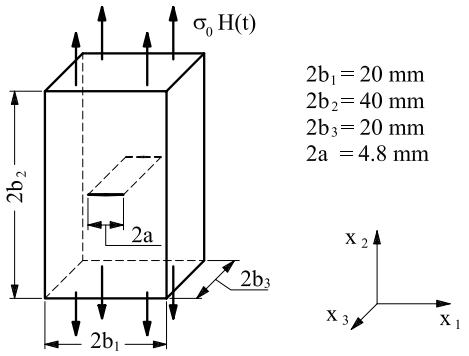

Fig. 6. Rectangular bar containing a central through-thickness crack.

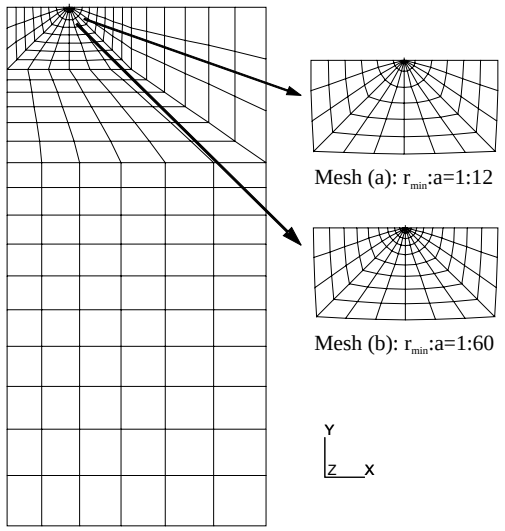

Fig. 7. FE-mesh of the central through-thickness crack in a rectangular bar.

the half crack length a is $r_{\min} : a = 1 : 12$. For mesh (b) it is $r_{\min} : a = 1 : 60$. The results for stress intensity factors $K_{\mathrm{I}}^{\mathrm{d}}(t)$ are plotted in Fig. 8 normalised with respect to $K_0 = \sigma_0\sqrt{\pi a}$. All three methods give similar graphs. It can be seen that the J-integral method is independent from the fineness of the finite element mesh. In each time step the J-integral was evaluated using several concentric integration domains around the crack tip. A sufficient convergence is found for four integration rings. The graphs of the MCCI and the DIM obviously depend on the size of the elements at the crack tip. The largest dependence was found for the DIM. The reason is, that the DIM and the MCCI are based on the asymptotic solution at the crack tip, which cannot be reproduced exactly by the regular finite elements used in the computation. Nevertheless, all results are within a range of ±5% with the J-integral taken as reference value. The normalised stress intensity factor computed with the J-integral method is compared in Fig. 9 with results by Fedelinski et al. (1995), who used a time domain method, a Laplace transform method and a dual reciprocity method. Furthermore, results by Chen (1975) are plotted, who calculated $K_{\mathrm{I}}^{\mathrm{d}}/K_0$ with a finite difference method. The results of the J-integral agree well with those of the other methods.

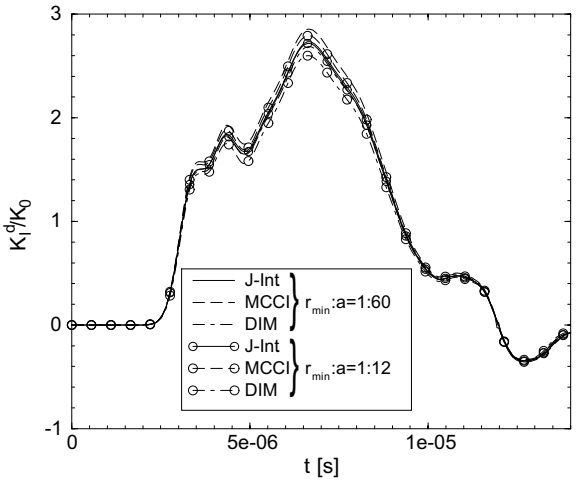

Fig. 8. Accuracy of different methods for the calculation of K_I^d depending on the mesh fineness at the crack tip.

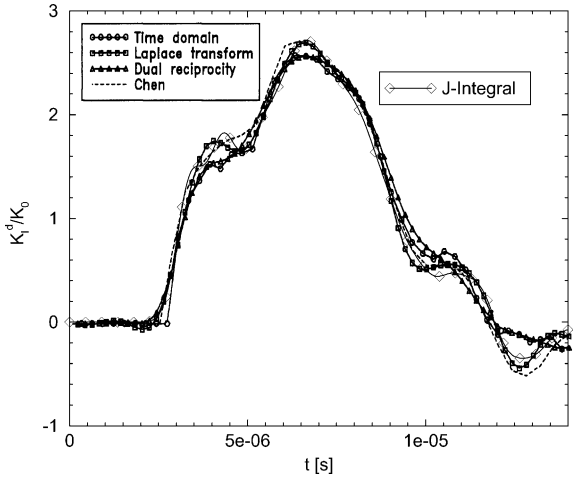

Fig. 9. Comparison of K_I^d/K_0 computed with the J-integral method with results from Fedelinski et al. (1995) and Chen (1975).

3.2. Central through-thickness crack in a rectangular bar, 3D-model

In order to study the distribution of the dynamic stress intensity factor along the crack front, a three-dimensional finite element model of the central through-thickness crack was analysed. It is based on mesh (a) in Fig. 6, which was extruded in the x_3-direction. K_I^d/K_0 is computed at all nodes along the crack front. In Fig. 10 the results of the J-integral method are plotted for three positions ($s = 0$, $s = b_3/2$, $s = b_3$) and compared with the two-dimensional solution. As can be seen, the dynamic stress intensity factor varies strongly along the crack front. The maximum of K_I^d is reached in the middle of the crack front ($s = b_3$) and lies approximately 20% above the maximum value of the 2D-solution. Next, the results of the J-integral method are compared to those obtained by the MCCI and the DIM. The corresponding graphs, plotted in Fig. 11 for $s = b_3$, agree well. At the maximum of K_I^d/K_0 the differences lie within 7%.

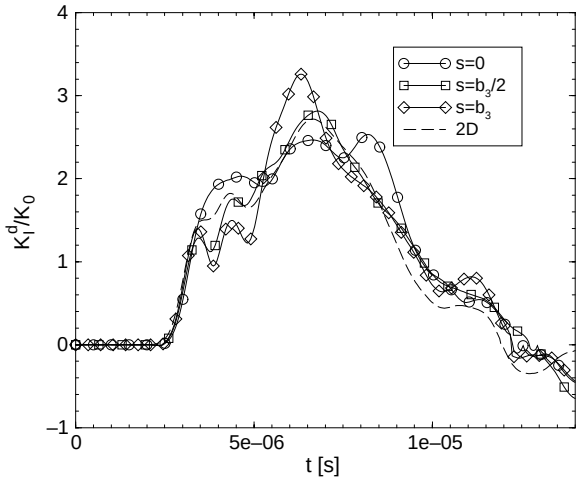

Fig. 10. Comparison of K_I^d/K_0 for the 3D-model and the 2D-model for the central through-thickness crack.

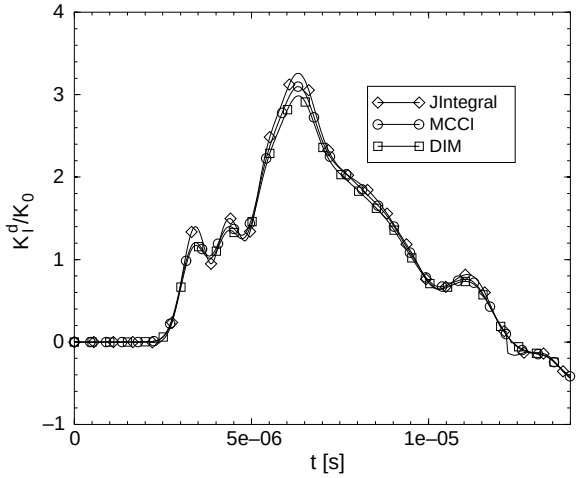

Fig. 11. Comparison of different methods for the calculation of K_I^d for the 3D-model of a central through-thickness crack ($s = b_3$).

3.3. Elliptical crack in a rectangular bar

As a second example a rectangular bar containing a central elliptical crack is considered. The dimensions of the bar are shown in Fig. 12 and the material constants are as follows: shear modulus $\mu = 77 \times 10^9$ Pa, density $\rho = 7900\ \mathrm{kg\,m^{-3}}$ and Poisson's ratio $\nu = 0.216$. The bar is subjected to an impact load $\sigma_0 H(t)$ at both ends. For the finite element simulation the model shown in Fig. 13 was used. It consists of 5790 elements, using 2304 elements in the region along the crack front. Taking advantage of all symmetries, only an eighth of the whole bar has to be modelled. The results for the J-integral method, the MCCI and the DIM are compared in Fig. 14. The dynamic stress intensity factor $K_I^d(t)$ is plotted for the minor axis of the elliptical crack and is normalised with respect to the static stress intensity factor K_I obtained by Newman and Raju (1981). Again, all three methods show a good agreement. However, the results will increasingly

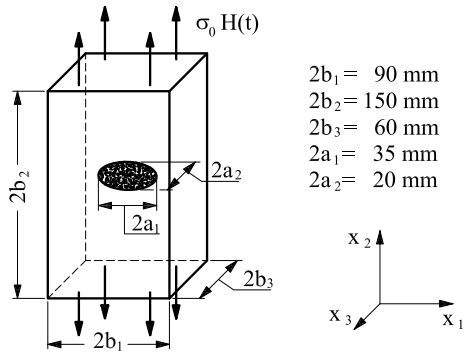

Fig. 12. Rectangular bar containing an elliptical crack.

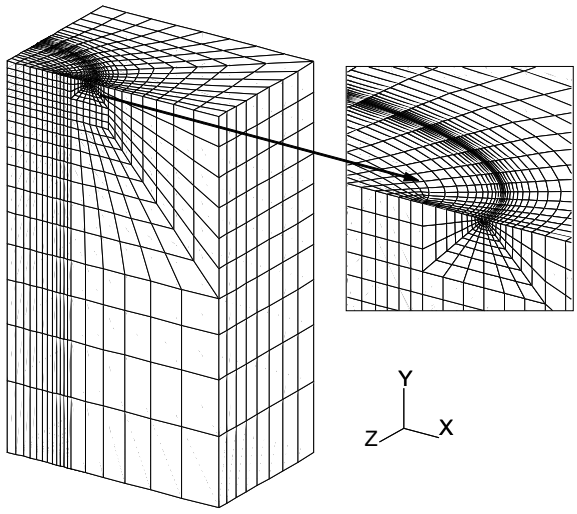

Fig. 13. FE-mesh of the elliptical crack in a rectangular bar.

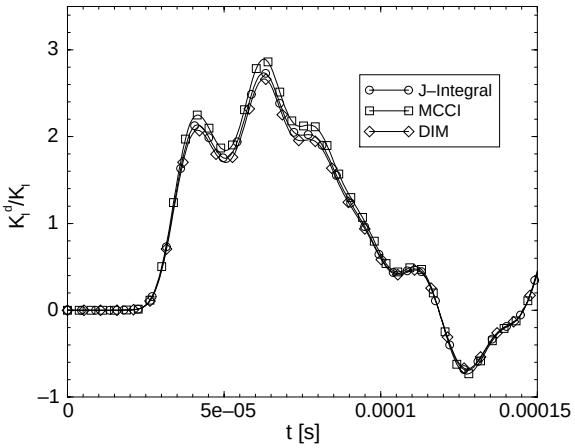

Fig. 14. Comparison of different methods to calculate K_I^d for an elliptical crack in a rectangular bar.

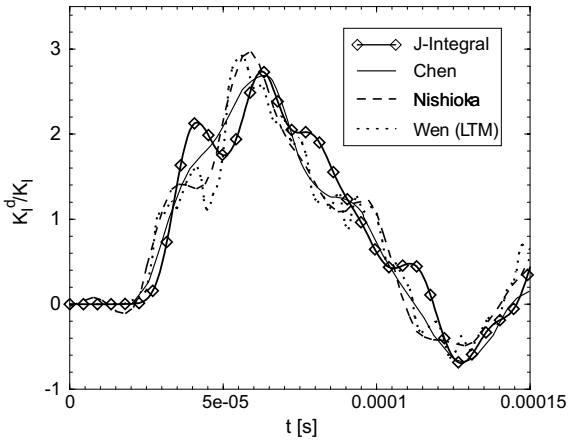

Fig. 15. Comparison of K_I^d/K_I computed with the J-integral method with results from Wen et al. (1999), Nishioka (1995) and Chen and Wilkins (1977).

diverge from each other, if the mesh width near the crack tip grows. As for the through-thickness crack the J-integral delivers the best results for coarse finite element meshes. The results of the DIM and the MCCI differ in the maximum of $K_I^d(t)/K_I \approx 4$–6% from the J-integral. A comparison of the results with other three-dimensional solutions found in the literature (Wen et al., 1999; Nishioka, 1995; Chen and Wilkins, 1977) is given in Fig. 15. Considering the overall response, our results agree well with the others. The maximum value of K_I^d/K_I coincides best with Chen's result, whereas the trend of the curve follows the results of Nishioka and Wen et al.

4. Conclusions

To calculate the dynamic stress intensity factor $K_I^d(t)$, three different methods have been developed as post-processors for finite element simulations. They have been applied to two- and three-dimensional crack models. The MCCI method and the DIM are based on relatively straightforward algorithms, which may be implemented with a comparably low effort, whereas the equivalent domain integral method for J needs a more sophisticated algorithm. All results have shown that the MCCI and the DIM lead to an acceptable accuracy compared to the J-integral method. For the models investigated in this paper the deviations are always below 7%. The accuracy of the MCCI and the DIM techniques clearly depends on the fineness of the finite element mesh, whereas the J-integral shows a neglectable dependence on the mesh width near the crack tip. Nevertheless, the compact MCCI and DIM are worthwhile and easy techniques for many fracture mechanics applications, provided that a sufficiently fine meshing of the crack front is realised. Despite of the good results obtained by the MCCI and the DIM, the advantages of the J-calculation by means of the equivalent domain integral are obvious. The little mesh dependence makes it a robust method which does not require an extremely fine discretisation around the crack. The results are most accurate, since the calculation of J^d is rarely influenced by the quality of the solution of the field problem in the vicinity of the crack front singularity. Due to the path independence, different integration domains produce identical results providing a useful means to verify the accuracy. The extension of all three techniques to analyse mixed mode dynamic crack problems is straightforward. Then, the MCCI and DIM deliver the dynamic stress intensity factors separated for each crack opening mode, whereas the J-integral method has the drawback that only the energy release rate can be computed. The great advantage of all three finite

element techniques presented here consists in their applicability to crack configurations in any structure of finite size with arbitrary dynamic loading conditions on the boundary, whereas other methods get difficulties with finite boundaries.

References

Aliabadi, M.H., 1995. Dynamic Fracture Mechanics. Computational Mechanics Publications, Southampton, UK and Boston, USA.
Anderson, T.L., 1995. Fracture Mechanics. CRC Press, Boca Raton, Ann Arbor, London, Tokyo.
Anon, 2000. ABAQUS/Explicit User's Manual, Version 6.1. Hibbitt, Karlsson & Sorensen, Inc., Pawtucket, USA.
Atkinson, C., Eshelby, J.D., 1968. Flow of energy into the tip of a moving crack. Int. J. Fracture Mech. 4, 3–8.
Buchholz, F.G., 1984. Improved formulae for the finite element calculation of the strain energy release rate by the modified crack closure integral method. In: Robinson, J. (Ed.), Accuracy, Reliability and Training in FEM Technology. Dorset.
Chen, Y.M., 1975. Numerical computation of dynamic stress intensity factors by a Lagrangian finite-difference method (the HEMP code). Engng. Fracture Mech. 7, 653–660.
Chen, Y.M., Wilkins, M.L., 1977. Numerical analysis of dynamic crack problems. In: Elastodynamic Crack Problems. Noordhoff, pp. 1–58.
Fedelinski, P., Aliabadi, M.H., Rooke, D.P., 1995. Boundary element formulations for the dynamic analysis of cracked structures. In: Aliabadi, M.H. (Ed.), Dynamic Fracture Mechanics. Computational Mechanics Publications, Southampton, UK and Boston, USA.
Fedelinski, P., Aliabadi, M.H., Rooke, D.P., 1996. Boundary element formulations for the dynamic analysis of cracked structures. Engng. Anal. Bound. Elem. 4 (1), 45–56.
Freund, L.B., 1972. Energy flux into the tip of an extending crack in an elastic solid. J. Elasticity 2, 341–349.
Gross, D., 1996. Bruchmechanik. Springer, Berlin, Heidelberg, New York.
Hellen, T.K., 1975. On the method of virtual crack extension. Comput. Meth. Appl. Mech. Engng. 12, 353–364.
Kostrov, B.V., Nikitin, L.V., 1970. Some general problems of mechanics of brittle fracture. Archwm. Mech. Stosow 22, 749–775.
Moran, B., Shih, C.F., 1987. Crack tip and associated domain integrals from momentum and energy balance. Engng. Fracture Mech. 27, 615–642.
Nakamura, T., Shih, C.F., Freund, L.B., 1986. Analysis of a dynamically loaded three-point-bend ductile fracture specimen. Engng. Fracture Mech. 25, 323–339.
Newman Jr., J.C., Raju, I.S., 1981. Stress intensity factor equations for cracks in three-dimensional finite bodies. NASA Technical Memorandum 83200, pp. 1–49.
Nishimura, N., Guo, Q.C., Kobayashi, S., 1987. Boundary integral equation methods in elastodynamic crack problems. In: Boundary Elements IX, vol. 2. Computational Mechanics Publications, Southampton, UK and Boston, USA.
Nishioka, T., 1995. Recent developments in computational dynamic fracture mechanics. In: Aliabadi, M.H. (Ed.), Dynamic Fracture Mechanics. Computational Mechanics Publications, Southampton, UK and Boston, USA.
Shih, C.F., Moran, B., Nakamura, T., 1986. Energy release rate along a three-dimensional crack front in a thermally stressed body. Int. J. Fracture 30, 79–102.
Wen, P.H., Aliabadi, M.H., Young, A., 1999. Dual boundary element methods for three-dimensional dynamic crack problems. J. Strain Anal. 34 (6), 373–394.